

## HOW LONG DOES A BURST BURST?

BIN-BIN ZHANG<sup>1</sup>, BING ZHANG<sup>2</sup>, KOHTA MURASE<sup>3</sup>, VALERIE CONNAUGHTON<sup>1</sup> AND MICHAEL S. BRIGGS<sup>1</sup>  
*Draft version October 30, 2018*

### ABSTRACT

Several gamma-ray bursts (GRBs) last much longer ( $\sim$  hours) in  $\gamma$ -rays than typical long GRBs ( $\sim$  minutes), and recently it was proposed that these “ultra-long GRBs” may form a distinct population, probably with a different (e.g. blue supergiant) progenitor than typical GRBs. However, *Swift* observations suggest that many GRBs have extended central engine activities manifested as flares and internal plateaus in X-rays. We perform a comprehensive study on a large sample of *Swift* GRBs with XRT observations to investigate GRB central engine activity duration and to determine whether ultra-long GRBs are unusual events. We define burst duration  $t_{\text{burst}}$  based on both  $\gamma$ -ray and X-ray light curves rather than using  $\gamma$ -ray observations alone. We find that  $t_{\text{burst}}$  can be reliably measured in 343 GRBs. Within this “good” sample, 21.9% GRBs have  $t_{\text{burst}} \gtrsim 10^3$  s and 11.5% GRBs have  $t_{\text{burst}} \gtrsim 10^4$  s. There is an apparent bimodal distribution of  $t_{\text{burst}}$  in this sample. However, when we consider an “undetermined” sample (304 GRBs) with  $t_{\text{burst}}$  possibly falling in the gap between GRB duration  $T_{90}$  and the first X-ray observational time, as well as a selection effect against  $t_{\text{burst}}$  falling into the first *Swift* orbital “dead zone” due to observation constraints, the intrinsic underlying  $t_{\text{burst}}$  distribution is consistent with being a single component distribution. We found that the existing evidence for a separate ultra-long GRB population is inconclusive, and further multi-wavelength observations are needed to draw a firmer conclusion. We also discuss the theoretical implications of our results. In particular, the central engine activity duration of GRBs is generally much longer than the  $\gamma$ -ray  $T_{90}$  duration and it does not even correlate with  $T_{90}$ . It would be premature to make a direct connection between  $T_{90}$  and the size of the progenitor star.

### 1. INTRODUCTION

A number of GRBs (namely, GRBs 101225A, 111209A, 121027A and the most recent GRB 130925A) were found to last much longer ( $\sim$  hours instead of tens of seconds) than typical GRBs (Levan et al. 2014; Gendre et al. 2013; Virgili et al. 2013; Stratta et al. 2013). Such “ultra-long” GRBs were also seen historically in BATSE and Konus-Wind data (see, e.g., Connaughton et al. 1997; Connaughton 1998; Giblin et al. 2002; Connaughton 2002; Nicastro et al. 2004; Levan et al. 2005; Pal’shin et al. 2008). Motivated by such long durations and other multi-wavelength properties (e.g., the faint host galaxy of GRB 101225A and its late time color consistency with SNe II), several groups (Levan et al. 2014; Gendre et al. 2013) have proposed that the unusually long durations of these GRBs may point towards a new type of progenitor stars with much larger radii, such as blue supergiants (Mészáros & Rees 2001; Nakauchi et al. 2013), in contrast to the well-accepted compact Wolf-Rayet star progenitor (Woosley & Bloom 2006). In this scenario, the stellar envelope of a large-radius massive star would fall back in an extended time scale to fuel the central engine and to power a relativistic jet. The expected cocoon emission can explain anomalies in the afterglow data (Nakauchi et al. 2013). If this is the case, then ultra-

long GRBs may form a distinct new population from the traditional short (compact star merger type) and long (Wolf-Rayet collapsar) GRBs.

However, careful studies based on many more criteria (other than duration alone) are needed to claim a new population. While the short and long dichotomy has long been known (Kouveliotou et al. 1993), it was not until the discoveries of the afterglow, redshift, and host galaxies of both types of events that a firm claim was made about their distinct progenitor types. Indeed, based on a dozen multi-wavelength observational criteria (Zhang et al. 2009), one was able to establish robust evidence that long (collapsar/magnetar type) and short (compact star merger type) GRBs are very different from each other, not only in duration, but also, more importantly, in their host galaxy types, specific star formation rate, supernova association, circumburst medium properties, spectral properties, empirical correlations, and derived jet opening angles. Any proposal to claim a new population of GRBs should be performed in a similar manner. Even though these multi-wavelength criteria are being paid attention to (e.g. Levan et al. 2014), a careful comparative study between the proposed “ultra-long” GRB population and the more classical long GRB population is needed.

Interestingly, not all claimed ultra-long GRBs have ultra-long durations in  $\gamma$ -rays. Only GRBs 111209A and 130925A have an exceedingly long  $\gamma$ -ray  $T_{90}$ , i.e.  $> 10000$  s (Golenetskii et al. 2011, ; Markwardt et al. 2013; Golenetskii et al. 2013). GRB 101225A was first measured to have a  $T_{90}$  of  $1088 \pm 20$  s (Palmer et al. 2010). Later studies measured a longer duration of up to 7000 s based on the analysis of gamma-ray data from BAT in subsequent *Swift* orbits (Thöne et al.

<sup>1</sup> Center for Space Plasma and Aeronomic Research (CSPAR), The University of Alabama in Huntsville, Huntsville, AL 35899, USA; binbin.zhang@uah.edu

<sup>2</sup> Department of Physics and Astronomy, University of Nevada, Las Vegas, Box 454002, 4505 Maryland Parkway, Las Vegas, NV 89154-4002, USA

<sup>3</sup> Hubble Fellow - Institute for Advanced Study, 1 Einstein Dr. Princeton, NJ 08540, USA

2012). The gamma-ray duration of GRB 121027A, on the other hand, is only  $62.6 \pm 4.8$  s in *Swift* /BAT band (Barthelmy et al. 2012), which is very typical for long GRBs. The main supportive evidence that GRBs 121027A and 101225A were included in the ultra-long category was their long-lasting highly-variable X-ray light curves (Levan et al. 2014). In other words, the “ultra-long” durations of GRBs 121027A (“ $T_{90}$ ”  $\sim$  6000s, Levan et al. 2014) and 101225A (“ $T_{90}$ ”  $\sim$  7000s, Levan et al. 2014) are both observed in the X-ray band other than being seen in  $\gamma$ -ray band only. In fact, *Swift* observations over the years have revealed that the GRB central engine lasts much longer than indicated by  $T_{90}$  (Zhang 2011), via the manifestation of both X-ray flares (Burrows et al. 2005; Zhang et al. 2006; Liang et al. 2006; Chincarini et al. 2007; Margutti et al. 2011) and the so-called “internal plateaus” – X-ray plateaus followed by an abrupt decay that cannot be interpreted with the external shock model (Troja et al. 2007; Liang et al. 2007). Some authors even suggested that the entire X-ray afterglow may be of an internal origin powered by central engine (Ghisellini et al. 2007; Kumar et al. 2008; Murase et al. 2011). The existence of an extended tail emission in most long GRBs was already hinted from the BATSE data through stacking long GRB light curves (Connaughton 2002). If we believe that GRB duration definition should invoke X-ray data, then the the duration distribution of GRBs should be re-analyzed in a systematical manner.

In this paper, we perform a comprehensive study of *Swift* XRT data, focusing on the long-term central engine activities in the X-ray light curves, to address typically how long a burst lasts, and whether the claimed ultra-long GRBs are special. In §2, we propose a new definition,  $t_{\text{burst}}$ , from the physical point of view, to measure the true time scale of the central engine activity. We also introduce quantitative observational criteria to measure  $t_{\text{burst}}$  from data. In §3, we use the *Swift* data to systematically derive  $t_{\text{burst}}$  and its distribution. We discuss the results and theoretical implications in §4.

## 2. $t_{\text{burst}}$ : MOTIVATION, DEFINITION AND CRITERIA

Mounting evidence supports the hypothesis that X-ray flares have the same intrinsic physical origin as  $\gamma$ -ray pulses, but just have a reduced flux and peak energy so that they can be below the sensitivity threshold of a  $\gamma$ -ray detector (Fig.1 for illustration). For extremely bright X-ray flares, the tips of the flares can be registered by the  $\gamma$ -ray detector, and hence, included in  $T_{90}$ . Figure 2 gives an example of a GRB (090715B) whose early X-ray flare as detected by *Swift* XRT (red) was also recorded by *Swift* BAT (blue), but the later extended X-ray flares were not. Therefore,  $T_{90}$  measurement is not a reliable quantity to describe how long a burst “bursts”.

In this Paper, we give a physically motivated definition of the duration of a GRB: *The burst duration  $t_{\text{burst}}$  is an observable quantity of a GRB, during which the observed ( $\gamma$ -ray and X-ray) emission is dominated by emission from a relativistic jet via an internal dissipation process (e.g. internal shocks or magnetic dissipation), not dominated by the afterglow emission from the external shock.*

This definition is different from the traditional  $T_{90}$  in that it considers multi-wavelength signatures in addition

to  $\gamma$ -rays. The rationale of using such a definition is illustrated in a cartoon picture in Fig.1. The GRB central engine continuously ejects energy but generally with a reduced power as a function of time. The peak energy of the spectrum  $E_p$  is positively correlated to its luminosity (e.g. Lu et al. 2012), so it decreases with time. At a certain epoch ( $\sim T_{90}$ ), the signal drops out from the  $\gamma$ -ray band, but it still continues in the X-ray band. On the other hand, the afterglow component sets in early on, peaking at  $t_{\text{ag},p}$  and decays with time. It is initially over-shone by the internal-origin X-ray component (X-ray flares and plateaus). Since the decay of internal emission is typically very steep, the afterglow component will eventually show up. The X-ray light curve therefore displays a steep-to-shallow transition when the external shock component emerges. In principle, the central engine can activate again to power bright internal emission to outshine the afterglow component again later. So a secure *lower limit* of the central engine activity time should be defined by the *last* observed steep-to-shallow transition, and this is our definition of  $t_{\text{burst}}$ .

Such a definition is however not easy to quantify. This is because in order to claim an internal origin of X-ray emission, theoretical modeling is needed to exclude an external shock origin of the observed flux. The standard external shock afterglow model (e.g. Gao et al. 2013 for a review) generally predicts broken-power-law light curves. The steepest decay can be achieved when the blastwave enters a void, during which emission is powered by the high-latitude emission (Zhang et al. 2007, 2009). The decay slope in this regime is  $\alpha = 2 + \beta$  (convention  $F_\nu \propto t^{-\alpha} \nu^{-\beta}$ ; Kumar & Panaitescu 2000), which is typically smaller than 3. Due to the equal-arrival-time surface effect, any variability in external shock emission should satisfy  $\Delta t/t \geq 1$ , where  $\Delta t$  and  $t$  are the variability time scale and the epoch of observation, respectively (e.g. Ioka et al. 2005). As a result, rapid variabilities with  $\Delta t/t \ll 1$  (as observed in X-ray flares) and any steep decay with slope steeper than -3 (as observed in “internal X-ray plateaus”) are deemed as due to an internal origin.

We therefore adopt the following procedure to define  $t_{\text{burst}}$  of a GRB: 1) Calculate  $T_{90}$  for the *Swift* /BAT light curve; 2) Fit the *Swift* /XRT light curve as a multi-segment broken power-law; 3) Identify the steep-to-shallow transitions in the light curve, and record the decay slope before the transition; 4) Identify the *last* transition with pre-break slope steeper than -3, and record the transition time<sup>4</sup>. The burst duration  $t_{\text{burst}}$  is defined as the maximum of this transition time and  $T_{90}$  of  $\gamma$ -ray emission<sup>5</sup>.

Notice that this method identifies only the X-ray emission that *must* be of an internal origin, but may not necessarily catch the full duration of internal emission if some internal-origin emission does not show such a steep decline (e.g. Ghisellini et al. 2007; Kumar et al. 2008;

<sup>4</sup> Qin et al. (2013) and Peng et al. (2013) also discussed GRB central engine time scale using the X-ray flare data. They used the peak of the last X-ray flare to define  $t_{\text{burst}}$ .

<sup>5</sup> Here it is assumed that emission during  $T_{90}$  is due to internal emission powered by central engine activity. This hypothesis is valid for most high-luminosity GRBs, which is supported by the observed rapid variability of the gamma-ray light curves as well as the X-ray follow-up steep decay phase following  $\gamma$ -ray emission.

Murase et al. 2011). Therefore, we may typically regard  $t_{\text{burst}}$  as the *lower limit* of GRB central engine activity.

### 3. OBSERVED $t_{\text{burst}}$ DISTRIBUTION

As of 2014 January 22nd, 712 GRBs have X-ray afterglows detected by *Swift* /XRT. All the XRT light curves are directly taken from the *Swift* /XRT team website<sup>6</sup> (Evans et al. 2009) at the UK *Swift* Science Data Centre (UKSSDC), which were processed using HEASOFT v6.12. Several example light curves are presented in Fig.3, including the four ultra-long GRBs and some typical GRBs with canonical X-ray light curve behavior. One can see that the central engine activity usually lasts much longer than  $T_{90}$ .

In order to measure  $t_{\text{burst}}$ , we use only well-sampled XRT light curves with late-time observations. We select a “good” sample based on the following criteria: (1) The X-ray light curve must have at least 6 data points, excluding upper limits; (2) The X-ray light curve has at least one steep-to-shallow transitions (with the steeper slope  $< -3$ ); or (3) if the X-ray light curve has no steep-to-shallow transition, the starting time of XRT observation,  $T_{X,0}$ , is smaller than  $T_{90}$ . For this latter case, we take  $T_{90}$  as  $t_{\text{burst}}$ . Our final good sample consists of 343 GRBs (Table 1). This “good” sample, despite having robust measurements of  $t_{\text{burst}}$ , is incomplete. A good fraction of GRBs (consisting of 304 GRBs), which we define as the “undetermined” sample, have at least 6 data points in the light curves, do not have a required steep-to-shallow transition (with steeper slope  $< -3$ ), but have an observational gap between  $T_{90}$  and  $T_{X,0}$ . The  $t_{\text{burst}}$  of these GRBs likely fall into the gap between  $T_{90}$  and  $T_{X,0}$ , but are not included in the “good” sample. Therefore the “good” sample is biased against GRBs with a short  $t_{\text{burst}}$ .

The essential part of measuring  $t_{\text{burst}}$  is to identify a shallower break feature in the late segments of the X-ray light curve. This is tricky, since late time X-ray data sometimes have too few photons, or the entire light curves lack time coverage<sup>7</sup>. To maximize the use of the observational data, we apply a multivariate adaptive regression splines technique (e.g., Fredman et al. 1991) to the observed light curves in the logarithmic scale, which can automatically detect and optimize breaks<sup>8</sup>. By measuring the decay slope before the break, one can judge whether the pre-break emission is internal, and hence, to measure  $t_{\text{burst}}$ . Figure 4 shows several examples of such measurements. In several cases (e.g., GRBs 130925A, 121027A, 111209A, 090715B and 051117A), such a break is clearly identified so that  $t_{\text{burst}}$  is measured. In a few cases (e.g., GRB 140102A), such a break is not identified, but there is overlap between  $\gamma$ -ray and X-ray observations, i.e.  $T_{X,0} < T_{90}$ . For these cases, we take  $t_{\text{burst}} = T_{90}$ . In some other cases (e.g. GRBs 101225A and 050724), the emergence of the external shock after-

glow component is lacking at the end of X-ray observation, so that only the lower limit of  $t_{\text{burst}}$  can be determined as the last XRT observation time. In some other cases (e.g. GRB 110503A), the X-ray light curve is dominated by the afterglow component from the beginning, and there is no overlap between  $T_{90}$  and the XRT observation, we thus *exclude* them in them good sample but include them into the undetermined sample.

The distribution of  $t_{\text{burst}}$  of the good sample is shown in Figure 5(a)<sup>9</sup>. The median value of  $t_{\text{burst}}$  of the good sample is 428 s, which is much longer than the peak of  $T_{90}$  distribution in previous works (e.g., about 20 s for the BATSE sample, Preece et al. 2000). Within the entire sample, about 25.6% GRBs have  $t_{\text{burst}} > 10^3$  s and 11.5% GRBs have  $t_{\text{burst}} > 10^4$  s. Interestingly we found the traditional short GRBs (with  $T_{90} \leq 2$  s) in our good sample have similar values of  $t_{\text{burst}}$  (blue solid line in Figure 5a) to long GRBs.

The distribution of the  $t_{\text{burst}}$  of the good sample can be fitted by a mixture of two normal distributions in log space<sup>10</sup>, with a narrow, significant peak at  $\sim 355$  s, and a wider, less significant peak at  $\sim 2.8 \times 10^4$  s respectively<sup>11</sup>.

As discussed above, this apparent bimodal distribution is subject to strong selection effects due to observational biases. In the following, we address two strong selection effects in turn.

- First, there is a *Swift* slewing gap between  $\gamma$ -ray observations (i.e.,  $T_{90}$ ) and the first XRT observation time,  $T_{X,0}$ . It is likely that  $t_{\text{burst}}$  falls into this gap for many GRBs in the undetermined sample (e.g. GRB 110503A in Figure 4). The inclusion of this sample (whose size is comparable to the good sample) would modify the  $t_{\text{burst}}$  distribution significantly. In order to check how this effect changes the  $t_{\text{burst}}$  distribution we perform the following tests:

(1) We simply let  $t_{\text{burst}} = T_{90}$  for the undetermined sample and plot the distribution of  $t_{\text{burst}}$  of the whole sample (good + undetermined) of 647 GRBs in Figure 5 (b). By doing so, the values of  $t_{\text{burst}}$  in the undetermined GRB sample could be underestimated, so that Figure 5 (b) may be still regarded as a biased illustration of the  $t_{\text{burst}}$  distribution. Under this treatment, these  $t_{\text{burst}}$  values are more consistent with a single component. However, a Gaussian model can only poorly fit the data: there appears a sudden drop of  $t_{\text{burst}}$  around 1000 s and a significant excess in the “ultra-long” regime with  $t_{\text{burst}} \geq 10^4$  s.

<sup>9</sup> The distribution of the  $t_{\text{burst}}$  of the real time Swift GRB sample, as well as the fitting result of each individual GRB, is available online at <http://grbscience.com/tburst.html>.

<sup>10</sup> We used the log-Normal function to model the  $t_{\text{burst}}$  components based on the facts that the burst duration likely depends on many physical parameters (e.g. mass, spinning velocity, metallicity of the progenitor star, total energy budget etc). Those parameters can easily play as product form into the function of the  $t_{\text{burst}}$  (see e.g., Zhang et al. 2009). Statistically speaking, if a parameter depends on the product of more than three random variables, then its distribution should be log-normal due to central limit theorem (see e.g., Aitchison & Brown 1957; Ioka & Nakamura 2002).

<sup>11</sup> We use software ‘mclust’, which is an R package for normal mixture modeling via expectation-maximization (EM) algorithm, to automatically identify the optimized mixture model. The best model is selected based on the Bayesian Information Criterion (BIC). For details, see <http://www.stat.washington.edu/mclust/>

<sup>6</sup> [http://www.Swift.ac.uk/xrt\\_curves/](http://www.Swift.ac.uk/xrt_curves/)

<sup>7</sup> A low Earth orbit satellite is subject to Earth occultation, which would affect detections of long-lived emission. This effect is discussed more in §4.

<sup>8</sup> Our results are consistent with the fitting results obtained by Evans et al. (2009) (see, e.g. [http://www.swift.ac.uk/xrt\\_live\\_cat/](http://www.swift.ac.uk/xrt_live_cat/)), but we do not exclude the steep decay and flare phases, which are essential to measure  $t_{\text{burst}}$

(2) By assuming  $T_{90} \leq t_{\text{burst}} \leq T_{X,0}$ , we generate a uniformly-distributed random value of  $t_{\text{burst}}$  between  $T_{90}$  and  $T_{X,0}$  in logarithmic scale and assign it to  $t_{\text{burst}}$  for each GRB in the undetermined sample. We then plot the  $t_{\text{burst}}$  distribution of the whole sample (good + undetermined) in Figure 5 (c). A Gaussian fit is improved, but the excess of the ultra-long GRBs still exists.

- There is an orbital gap around thousands of seconds (Fig.4, e.g. GRB 110503A) due to various reasons such as geometry configuration between *Swift* orbital position relative to the GRB source position which is subject to Sun, Moon and Earth observation constraints, instrumental temperature of *Swift*, and delay of observation in respect to the priority of other ongoing (Target of Opportunities (ToOs)). All these factors act as a selection effect against finding  $t_{\text{burst}}$  values within this gap. This gap (starting from  $t_{\text{gap},1}$  and ending at  $t_{\text{gap},2}$ , which are measured in the observed light curves, see e.g. GRB 110503A in Figure 5) has a typical value of  $\sim 3200$  s (Figure 6a). The existence of such a gap has two effects on the  $t_{\text{burst}}$  distribution. First, if  $t_{\text{burst}}$  falls into this gap, these values are not registered, so that one would expect a dip in the  $t_{\text{burst}}$  distribution. Second, for those bursts whose real  $t_{\text{burst}}$  falls into this gap, one would mistakenly take an earlier steep-to-shallow transition break as  $t_{\text{burst}}$ , giving rise to a pile-up effect before the beginning of the orbital gap (see Figure 6b), which may be responsible for the sharp drop of the  $t_{\text{burst}}$  distribution around 1000 s in Fig.5(b). In order to test these speculations, we perform a Monte-Carlo simulation by assuming that the intrinsic  $t_{\text{burst,int}}$  distribution is a single-peak Gaussian distribution in logarithmic space. Guided by the fit in Figure 5(c), we assume that the Gaussian distribution has a mean value  $\mu = \log t_{\text{burst,int}} = 2.2$  and a standard deviation  $\sigma = 0.6$ . We generate  $10^4$  GRBs whose  $t_{\text{burst,int}}$  follows such a distribution as shown in Figure 7(a). Each simulated GRB has a parameter set of  $\{t_{\text{burst,int}}, T_{90}, t_{\text{gap},1}, t_{\text{gap},2}\}$ , where  $T_{90}, t_{\text{gap},1}, t_{\text{gap},2}$  are generated following their corresponding observed distributions, as shown in Figure 7(b) and Figure 7(c). To take account of the orbital gap effect, we check whether each  $t_{\text{burst,int}}$  falls into the gap between  $t_{\text{gap},1}$  and  $t_{\text{gap},2}$  for each simulated GRB. If not, we take the “observed” value  $t_{\text{burst}} = t_{\text{burst,int}}$ . If yes, we then assign  $t_{\text{burst}}$  a random value between  $T_{90}$  and  $t_{\text{gap},1}$  in the logarithmic scale. The distribution of the final simulated  $t_{\text{burst}}$  is shown as the solid line in Figure 7(d), where the intrinsic input distribution is also plotted as the red dotted histogram. The resulting simulated  $t_{\text{burst}}$  distribution shows a significantly sharp drop around 1000-3000 s as well as dip afterwards. All these signatures are similar to the  $t_{\text{burst}}$  distributions derived from the data (Fig.5(a-c)). Our simulation suggests that the hypothesis of one single  $t_{\text{burst}}$  distribution component cannot be ruled out by the data.

#### 4. SUMMARY AND THEORETICAL IMPLICATIONS

In this paper, we investigate the true GRB central engine activity duration distribution by considering both  $\gamma$ -ray and X-ray data. By defining  $t_{\text{burst}}$  based on some physically motivated criteria, we robustly derived  $t_{\text{burst}}$  for 343 GRBs. The  $t_{\text{burst}}$  distribution of this “good” sample shows an apparent bimodal distribution. If this is true, ultra-long GRBs could be more common than suggested in the literature (e.g., Levan et al. 2014). However, by including a larger sample whose  $t_{\text{burst}}$  values are not measured but can be guessed (303 GRBs in the “undetermined” sample) and by addressing two important selection effects, we found that the intrinsic  $t_{\text{burst}}$  distribution can be consistent with one single component. The existence of a separate “ultra-long” category of GRBs (Levan et al. 2014; Gendre et al. 2013; Boer et al. 2013) is neither required nor excluded by the data. Our results suggest that the ultra-long GRBs could be just a tail of a single long-duration GRB sample (see also Virgili et al. 2013).

As shown in Figure 8, our result indicates that a large fraction of long GRBs are actually quite long, even though their  $T_{90}$ 's are not extremely long. Evidence that two such long GRBs (030329 and 130427A) have associated Type Ic supernovae (Stanek et al. 2003; Hjorth et al. 2003; Xu et al. 2013) suggest that their progenitor is likely a Wolf-Rayet star whose hydrogen and helium envelopes have been depleted. The fact that their  $T_{90}$ 's are much longer than 10 s, the typical time scale for the jet to penetrate through the stellar envelope, suggests that the burst duration is not necessarily related to the size of the progenitor. Hence, making a direct connection between ultra-long GRBs and blue supergiants progenitor lacks strong physical justification. Theoretical investigations show that it becomes much more difficult for a jet to successfully penetrate through the stellar envelope of a blue supergiant, so that a significant fraction of such collapsing stars may just lead to failed GRBs (Murase & Ioka 2013). Also, blue supergiants are very unstable and short-lived, and their final explosion properties, including the possibility of launching a jet remain unclear.

How to prolong a GRB central engine duration with a compact progenitor star is an open question. For variable emission such as X-ray flares, fragmentation in the massive star envelope (King et al. 2005), fragmentation in the accretion disk (Perna et al. 2006), and the formation of a magnetic barrier around the accretor (Proga & Zhang 2006) have been proposed. If the engine is a millisecond magnetar instead of a black hole, the magnetic activity of the millisecond magnetar can power an extended emission (Metzger et al. 2011). The steady spin down of the magnetar (Zhang & Mészáros 2001) would also power an internal X-ray plateau (Troja et al. 2007). Alternatively, fall-back accretion of the stellar envelope onto a newly formed black hole (Kumar et al. 2008; Wu et al. 2013) can also make extended internal X-ray emission. All these mechanisms could also be applied to ultra-long GRBs without invoking a large progenitor star.

The wide peak of ultra-long GRB components may be also understood in a scenario where those GRB progenitor stars have a distribution of mass and size, ranging from Wolf-Rayet stars to blue supergiants. Further multi-wavelength data, especially the properties of as-

sociated SNe and host galaxies of GRBs with different  $t_{\text{burst}}$ , are needed to make further progress.

Bromberg et al. (2013) found a plateau in the  $dN/dT_{90}$  distribution in the BATSE, *Swift* and *Fermi* GBM samples, and argued that it provides direct evidence of the collapsar model. Realizing that  $T_{90}$  is no longer a good indication of central engine activity time scale, we apply our  $t_{\text{burst}}$  data in the good sample to carry out a  $dN/dt_{\text{burst}}$  analysis. The plateau found by Bromberg et al. using  $T_{90}$  is not reproduced with  $t_{\text{burst}}$  (Figure 9). Admittedly, the jet power in most GRBs reduces with time, and the most energy is still released during  $T_{90}$ . In any case, the collapsar signature suggested by Bromberg et al. (2013) may need further investigation.

We thank an anonymous referee for thoughtful comments, and David N. Burrows, Peter Mészáros, Xiao-Hong Zhao, Peter Veres, Kazumi Kashiyama, Xue-Wen Liu, Derek Fox and Shaolin Xiong for helpful discussion and suggestions. We thank Dirk Grupe for the information about *Swift* operations. BBZ thanks Jason Rudy for helpful comments on the codes of multivariate adaptive regression splines fitting. This work was partially supported by NASA /Fermi GI grant/ NNX11AO19G (BBZ). B.Z. acknowledges support from NASA NNX10AP53G. KM acknowledges the support by NASA through a Hubble Fellowship, Grant No. 51310.01 awarded by the STScI, which is operated by the Association of Universities for Research in Astronomy, Inc., for NASA, under Contract No. NAS 5-26555. We acknowledge the use of public data from the *Swift* data archive. *Facilities: Swift*.

## REFERENCES

- Aitchison, J. and Brown, J.A.C., 1957, The Log-normal Distribution. Cambridge (UK): Cambridge University Press.
- Barthelmy, S. D., Baumgartner, W. H., Cummings, J. R., et al. 2012, GRB Coordinates Network, 13910, 1
- Boer, M., Gendre, B., & Stratta, G. 2013, arXiv:1310.4944
- Bromberg, O., Nakar, E., Piran, T., & Sari, R. 2013, ApJ, 764, 179
- Burrows, D. N., Romano, P., Falcone, A., et al. 2005, Science, 309, 1833
- Chincarini, G. 2007, ApJ, 671, 1903
- Connaughton, V. 1998, in Eighteenth Texas Symposium on Relativistic Astrophysics, 514
- Connaughton, V. 2002, ApJ, 567, 1028
- Connaughton, V., Kippen, R. M., Preece, R. D., & Hurley, K. 1997, IAU Circ., 6785, 1
- Evans, P. A., Beardmore, A. P., Page, K. L., et al. 2009, Monthly Notices of the Royal Astronomical Society, 397, 1177
- Friedman, Jerome H. Multivariate Adaptive Regression Splines. The Annals of Statistics 19 (1991), no. 1, 1–67. doi:10.1214/aos/1176347963. http://projecteuclid.org/euclid.aos/1176347963.
- Gao, H., Lei, W.-H., Zou, Y.-C., Wu, X.-F., Zhang, B. 2013, New Astron. Rev., in press (arXiv:1310.2181)
- Gendre, B., Stratta, G., & collaboration, o. b. o. t. F. 2013, arXiv.org, 1305.3194v1
- Ghisellini, G., Ghirlanda, G., Nava, L., & Firmani, C. 2007, ApJ, 658, L75
- Giblin, T. W., Connaughton, V., van Paradijs, J., et al. 2002, ApJ, 570, 573
- Golenetskii, S., Aptekar, R., Mazets, E., et al. 2011, GRB Coordinates Network, 12663, 1
- Grupe, D., Nousek, J. A., Verres, P., Zhang, B.-B., & Gehrels, N. 2013, arXiv.org, 1305.3236v1
- Hjorth, J., Sollerman, J., Møller, P., et al. 2003, Nature, 423, 847
- Ioka, K., & Nakamura, T. 2002, ApJ, 570, L21
- Ioka, K., Kobayashi, S., & Zhang, B. 2005, ApJ, 631, 429
- King, A., O’Brien, P. T., Goad, M. R., Olsson, E., & Page, K. 2005, ApJ, 630, L113
- Kouveliotou, C., Meegan, C. A., Fishman, G. J., et al. 1993, ApJ, 413, L101
- Kumar, P., Narayan, R., & Johnson, J. L. 2008, Monthly Notices of the Royal Astronomical Society, 388, 1729
- Kumar, P., & Panaitescu, A. 2000, ApJ, 541, L51
- Knuth, D. E. 2000, arXiv:cs/0011047
- Levan, A., Nugent, P., Fruchter, A., et al. 2005, ApJ, 624, 880
- Levan, A. J., Tanvir, N. R., Starling, R. L. C., et al. 2014, ApJ, 781, 13
- Liang, E. W., Zhang, B. B., & Zhang, B. 2007, ApJ, 670, 565
- Liang, E. W., Zhang, B., O’Brien, P. T., et al. 2006, ApJ, 646, 351
- Lu, R.-J., Wei, J.-J., Liang, E.-W., et al. 2012, ApJ, 756, 112
- Margutti, R., Bernardini, G., Barniol Duran, R., Guidorzi, C., Shen, R. F., Chincarini, G. 2011, MNRAS, 410, 1064
- Mészáros, P., & Rees, M. J. 2001, ApJ, 556, L37
- Metzger, B. D., Giannios, D., Thompson, T. A., Bucciantini, N., & Quataert, E. 2011, MNRAS, 413, 2031
- Muggeo, V. M. R. 2003, Statistics in Medicine, 22, 3055
- , 2008, R News, 8, 20
- Murase, K., & Ioka, K. 2013, Physical Review Letters, 111, 121102
- Murase, K., Toma, K., Yamazaki, R., & Meszaros, P. 2011, The Astrophysical Journal, 732, 77
- Nakauchi, D., Kashiyama, K., Suwa, Y., & Nakamura, T. 2013, eprint arXiv:1307.5061
- Nicastro, L., Zand, J. J. M. i., Amati, L., et al. 2004, A&A, 427, 445
- Palmer, D. M., Barthelmy, S. D., Baumgartner, W. H., et al. 2010, GRB Coordinates Network, 11500, 1
- Pal’shin, V., Aptekar, R., Frederiks, D., et al. 2008, in GAMMA-RAY BURSTS 2007: Proceedings of the Santa Fe Conference (AIP), 117–120
- Peng, F.-k., Hu, Y.-D., Xi, S.-Q., et al. 2013, arXiv.org, 1302.4876
- Perna, R., Armitage, P. J., & Zhang, B. 2006, ApJ, 636, L29
- Preece, R. D., Briggs, M. S., Mallozzi, R. S., et al. 2000, The Astrophysical Journal Supplement Series, 126, 19
- Proga, D., & Zhang, B. 2006, MNRAS, 370, L61
- Qin, Y., Liang, E. W., Liang, Y.-F., et al. 2013, The Astrophysical Journal, 763, 15
- Stanek, K. Z., Matheson, T., Garnavich, P. M., et al. 2003, ApJ, 591, L17
- Stratta, G., Gendre, B., Atteia, J. L., et al. 2013, ArXiv e-prints, astro-ph.HE, 1306.1699
- Thöne, C. C., de Ugarte Postigo, A., Fryer, C. L., et al. 2012, Nature, 482, 120
- Troja, E., Cusumano, G., O’Brien, P. T., et al. 2007, ApJ, 665, 599
- Virgili, F. J., Mundell, C. G., Palshin, V., et al. 2013, ArXiv e-prints, astro-ph.HE, 1310.0313
- Woosley, S. E., & Bloom, J. S. 2006, ARA&A, 44, 507
- Wu, X.-F., Hou, S.-J., & Lei, W.-H. 2013, The Astrophysical Journal Letters, 767, L36
- Xu, D., de Ugarte Postigo, A., Leloudas, G., et al. 2013, The Astrophysical Journal, 776, 98
- Zhang, B. 2011, Comptes Rendus Physique, 12, 206
- Zhang, B., Fan, Y. Z., Dyks, J., et al. 2006, ApJ, 642, 354
- Zhang, B., & Mészáros, P. 2001, ApJ, 552, L35
- Zhang, B., Zhang, B.-B., Virgili, F. J., et al. 2009, ApJ, 703, 1696
- Zhang, B.-B., Liang, E.-W., & Zhang, B. 2007, ApJ, 666, 1002
- Zhang, B.-B., Zhang, B., Liang, E.-W., & Wang, X.-Y. 2009, ApJ, 690, L10

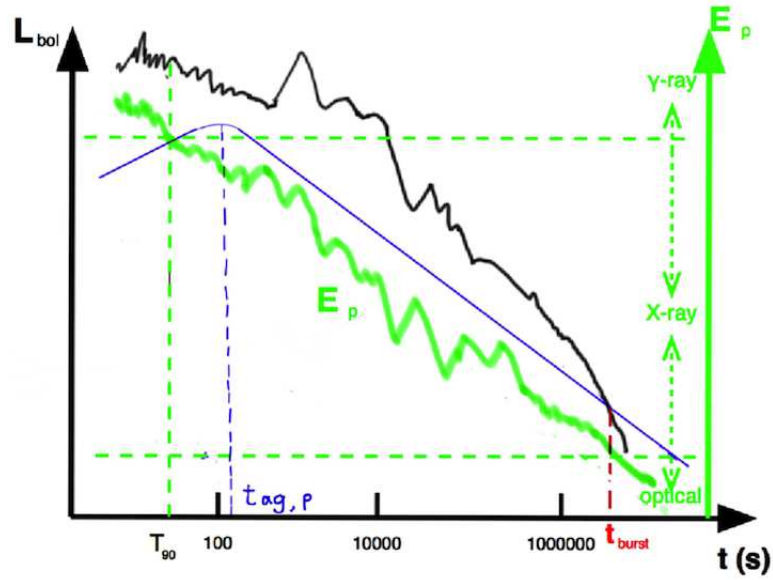


**Figure 1.** A sketch of the physical picture of GRB internal and external emission. The black curve denotes the bolometric internal emission light curve. The green solid curve denotes  $E_p$  evolution of the internal emission, indicating that the internal emission is initially in the  $\gamma$ -ray band, but shifts to X-rays later. The blue curve represents the external-shock afterglow emission component, which peaks at  $t_{ag,p}$  and becomes dominant at  $t > t_{burst}$ .

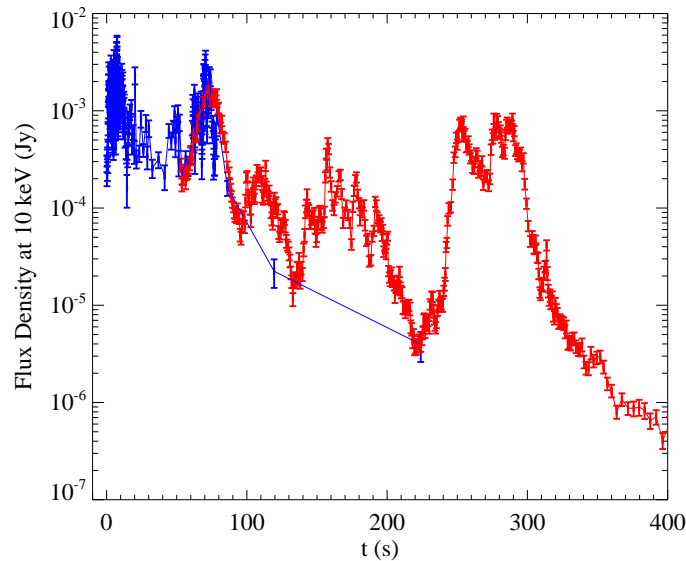


**Figure 2.** An example (GRB 090715B) that shows the similarity of X-ray flares (red data points) and prompt  $\gamma$ -ray emission (blue data points). The  $T_{90}$  of this GRB is 266 s, while  $t_{burst}$ , determined by X-ray data, is  $373 \pm 3$  s. Data are taken from [http://www.swift.ac.uk/burst\\_analyser/00357512/](http://www.swift.ac.uk/burst_analyser/00357512/), where the BAT and XRT data are extrapolated to the common energy band (10 keV) using their spectral information, respectively.

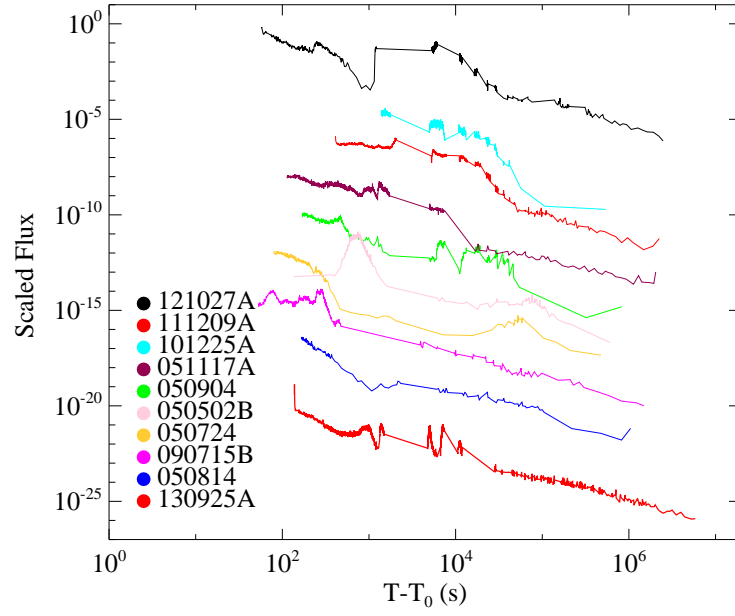


**Figure 3.** A comparison of  $\gamma$ /X-ray emission light curves of some GRBs, including the claimed four ultra-long GRBs and some others. Two other GRBs (050904 and 051117A) also show very similar features as the four events, suggesting that the so-called “ultra-long” GRBs may not be rare events. They are likely the extreme cases of normal GRBs with bright extended central engine activity emission.

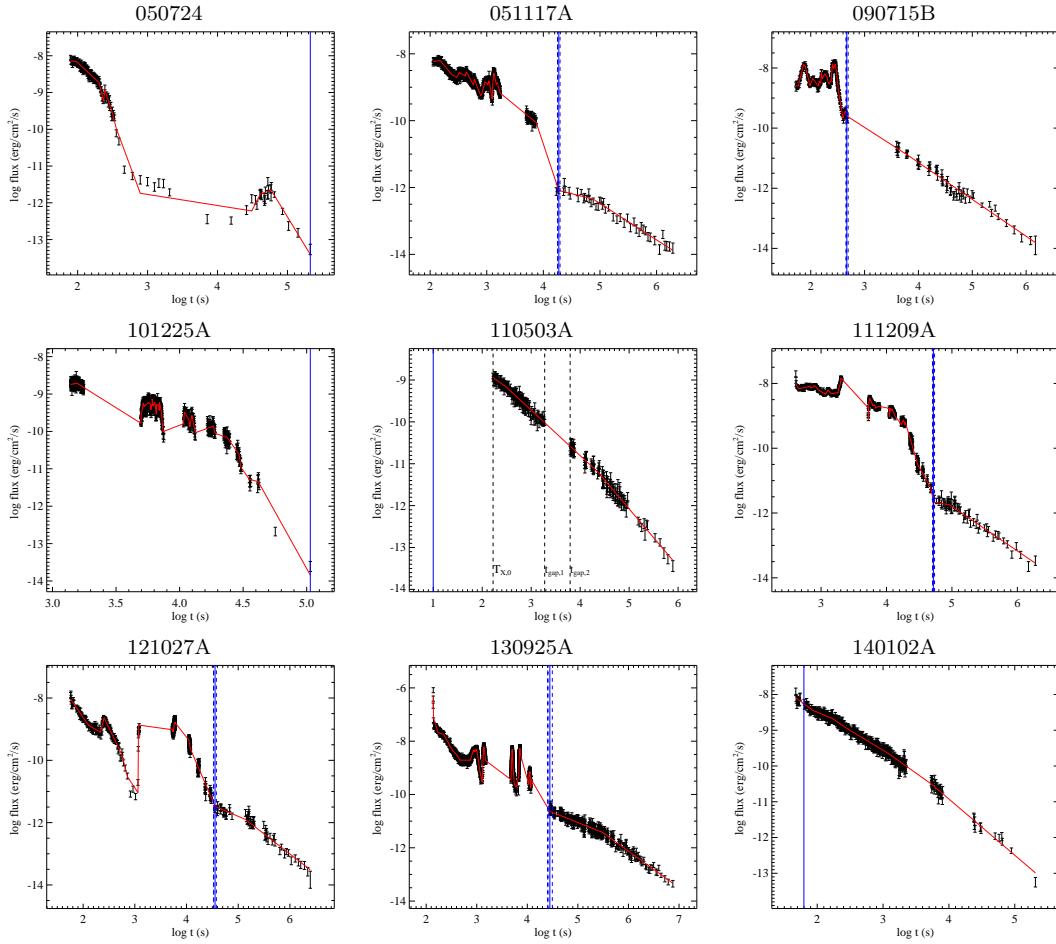


**Figure 4.** Some examples to show how to constrain  $t_{\text{burst}}$  with the XRT data. Black points are *Swift* /XRT observations. Red solid line represents the multi-segment broken power-law model fitted to the data. Blue solid line indicates the location of  $t_{\text{burst}}$ , and blue dashed lines (if available) represent the  $1\sigma$  uncertainty of  $t_{\text{burst}}$ . Note that GRB 110503A is not included in the good sample but is in the undetermined sample; see §4 for details. Data (0.3–10 keV energy flux) are taken from [http://www.swift.ac.uk/xrt\\_curves/](http://www.swift.ac.uk/xrt_curves/).

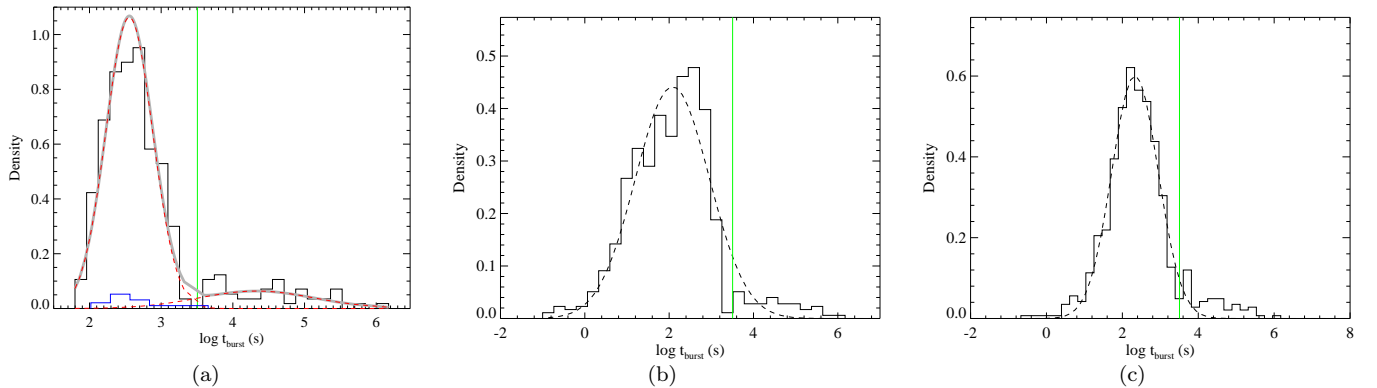


**Figure 5.** (a) The derived distribution of  $t_{\text{burst}}$  of the good sample (343 GRBs). The histogram bin sizes are optimized using Knuth’s rule (Knuth 2000). The vertical axis “density” is defined as “count/bin size/total count”. The derived  $t_{\text{burst}}$  are plotted as a black solid histogram. The distribution of the short GRBs ( $T_{90} < 2\text{s}$ ) in the good sample is plotted as the blue solid histogram. The fit result by a two-component Gaussian distribution is plotted as a thick grey solid line and each component is plotted as red dashed lines. A typical value of  $t_{\text{gap},2} - t_{\text{gap},1} = 3200\text{ s}$  is plotted as a vertical green solid line. (b) Distribution of  $t_{\text{burst}}$  for the good sample (343 GRBs) and the uncertain sample (304 GRBs), with  $t_{\text{burst}}$  of the uncertain sample set to  $T_{90}$ . (c) Same as (b), but with  $t_{\text{burst}}$  in the uncertain sample set to a uniformly-distributed random value between  $T_{90}$  and  $T_{X,0}$  in logarithmic scale.



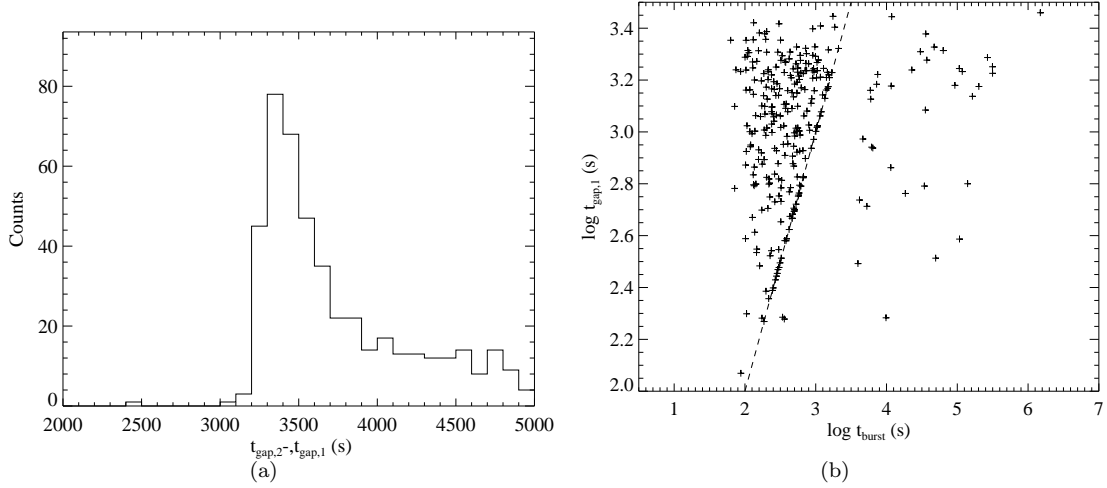


**Figure 6.** (a) Distribution of gap times in the XRT observations of the bursts in our sample  $t_{gap,2} - t_{gap,1}$ .  $t_{gap,1}$  is the start of the gap,  $t_{gap,2}$  is the end; (b) comparison between  $t_{burst}$  between  $t_{gap,1}$ , which shows most  $t_{burst}$  are measured before  $t_{gap,1}$ .

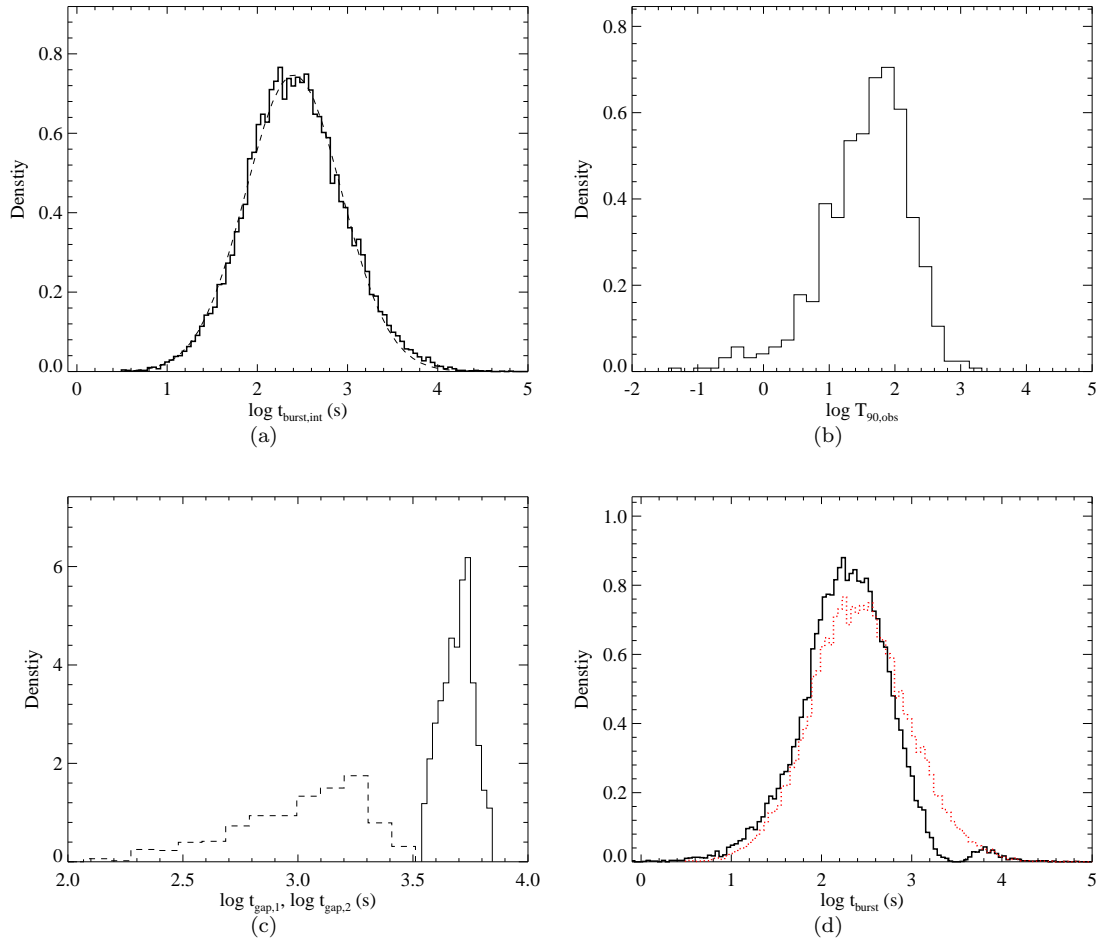


**Figure 7.** (a) Assumed intrinsic  $t_{burst,int}$  distribution, which is a Gaussian distribution in log scale with a mean value  $\mu = 2.2$  and a standard deviation  $\sigma=0.6$ ; (b) distribution of the observed  $T_{90}$  of the 647 GRBs in the full sample; (c) distributions of the observed  $t_{gap,1}$ ,  $t_{gap,2}$ ; (d) distribution of the simulated “observed” value  $t_{burst}$ . The intrinsic distribution is also plotted as the red dotted histogram for comparison.

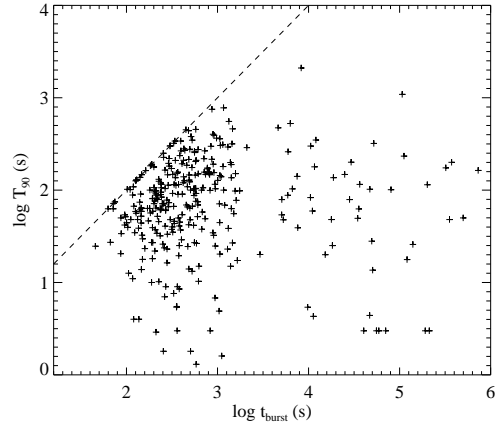


**Figure 8.**  $T_{90}$  vs  $t_{burst}$  for all the bursts in our sample. The dashed line marks where  $T_{90}=t_{burst}$ .

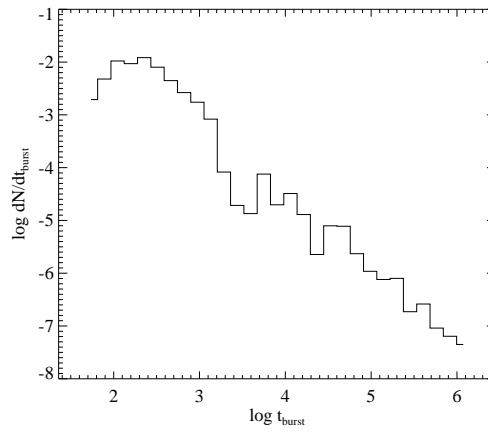


**Figure 9.** The  $dN/dt_{burst}$  diagram, which does not show an apparent plateau as suggested by Bromberg et al. (2013).

**Table 1**  
 $t_{\text{burst}}$  of the each GRB in our good sample

GRB	$\log t_{\text{burst}}$	GRB	$\log t_{\text{burst}}$	GRB	$\log t_{\text{burst}}$	GRB	$\log t_{\text{burst}}$	GRB	$\log t_{\text{burst}}$
	[s]		[s]		[s]		[s]		[s]
140114A	2.846±0.015	140108A	2.119±0.009	140102A	~1.798( $T_{90}$ )	131127A	2.574±0.027	131117A	2.475±0.048
131105A	2.527±0.014	131103A	3.268±0.021	131030A	2.377±0.003	131024B	2.519±0.086	131018A	2.463±0.022
131002B	2.373±0.019	131002A	1.939±0.021	130925A	4.066±0.002	130907A	2.990±0.004	130831B	2.935±0.027
130831A	2.221±0.050	130807A	3.596±0.041	130803A	2.155±0.029	130722A	2.624±0.005	130716A	2.175±0.142
130615A	3.175±0.044	130612A	2.032±0.039	130609B	2.625±0.005	130609A	2.121±0.068	130608A	2.774±0.033
130606A	2.697±0.008	130605A	2.023±0.037	130529A	~2.107( $T_{90}$ )	130528A	3.147±0.016	130527A	2.407±0.024
130514A	2.744±0.016	130505A	2.509±0.008	130427B	2.288±0.017	130427A	~2.212( $T_{90}$ )	130418A	~2.477( $T_{90}$ )
130408A	4.694±0.039	130327A	2.422±0.044	130315A	3.618±0.162	130211A	2.580±0.019	130131B	2.481±0.045
130131A	2.780±0.025	121229A	2.823±0.010	121217A	3.066±0.004	121212A	3.018±0.029	121211A	2.465±0.016
121128A	2.204±0.015	121125A	2.138±0.045	121123A	2.979±0.028	121108A	2.375±0.016	121102A	2.016±0.042
121031A	2.374±0.028	121027A	4.549±0.020	121024A	2.510±0.028	121001A	~2.167( $T_{90}$ )	120922A	2.868±0.037
120811C	2.306±0.021	120804A	2.019±0.048	120729A	~1.854( $T_{90}$ )	120728A	3.022±0.051	120724A	2.282±0.085
120703A	2.007±0.042	120701A	2.731±0.046	120612A	3.777±0.035	120521C	2.576±0.051	120521B	2.440±0.037
120521A	>2.513	120514A	2.409±0.009	120422A	2.701±0.050	120401A	3.183±0.082	120328A	2.191±0.016
120327A	2.238±0.041	120326A	2.429±0.020	120324A	2.377±0.012	120320A	≥5.146	120308A	4.555±0.151
120219A	2.756±0.053	120215A	2.604±0.068	120213A	2.436±0.030	120211A	2.381±0.099	120119A	4.478±0.031
120118B	2.414±0.036	120116A	2.445±0.026	120106A	2.151±0.037	111229A	>4.266	111228A	2.571±0.055
111225A	~2.029( $T_{90}$ )	111215A	3.165±0.005	111209A	4.801±0.025	111208A	≥4.606	111123A	2.937±0.011
111121A	~2.076( $T_{90}$ )	111107A	2.769±0.045	111103B	2.562±0.003	111022B	2.609±0.049	111016A	3.790±0.029
111008A	2.475±0.023	110921A	2.957±0.029	110915A	2.784±0.014	110820A	2.747±0.043	110818A	3.243±0.032
110808A	2.699±0.039	110801A	2.902±0.027	110726A	2.338±0.040	110709A	2.001±0.011	110709B	3.179±0.002
110420A	2.329±0.024	110414A	2.871±0.034	110411A	2.307±0.016	110407A	3.024±0.044	110319A	2.167±0.024
110312A	2.508±0.041	110223B	3.860±0.024	110213A	2.122±0.017	110210A	2.953±0.075	110205A	2.861±0.008
110119A	2.677±0.006	110102A	2.735±0.024	101225A	≥5.028	101219A	2.455±0.079	101213A	~2.130( $T_{90}$ )
101030A	2.735±0.031	101023A	2.240±0.007	101017A	2.824±0.029	101011A	~1.854( $T_{90}$ )	100915A	~2.301( $T_{90}$ )
100906A	≥5.304	100905A	2.900±0.030	100902A	≥6.173	100901A	2.771±0.029	100823A	2.232±0.065
100816A	2.351±0.047	100814A	2.738±0.016	100807A	2.419±0.042	100805A	2.543±0.014	100802A	3.666±0.102
100728A	2.969±0.015	100727A	2.742±0.011	100725B	2.779±0.021	100725A	~2.149( $T_{90}$ )	100704A	2.665±0.014
100621A	2.503±0.013	100619A	3.194±0.008	100615A	2.134±0.075	100614A	2.795±0.065	100606A	~2.681( $T_{90}$ )
100526A	2.737±0.023	100522A	2.055±0.083	100514A	2.646±0.024	100513A	2.760±0.037	100504A	2.702±0.023
100425A	2.672±0.034	100420A	2.661±0.118	100418A	2.500±0.033	100413A	2.490±0.017	100316D	~3.114( $T_{90}$ )
100305A	2.389±0.014	100302A	3.110±0.022	100219A	≥5.070	100212A	2.876±0.008	100205A	≥3.115
100117A	≥3.222	091221	2.398±0.043	091130B	2.335±0.028	091127	3.745±0.700	091104	2.918±0.059
091029	2.279±0.036	091026	2.737±0.010	091020	2.069±0.025	090929B	~2.556( $T_{90}$ )	090926B	~2.040( $T_{90}$ )
090926A	4.714±0.018	090912	2.988±0.039	090904B	2.162±0.027	090904A	3.002±0.024	090812	2.518±0.012
090809	3.993±0.036	090807	3.875±0.020	090728	2.272±0.072	090727	~2.480( $T_{90}$ )	090715B	2.671±0.005
090709A	2.105±0.013	090621A	2.851±0.046	090618	2.481±0.008	090530	2.117±0.043	090529	3.067±0.038
090519	2.729±0.047	090516	2.764±0.014	090515	≥2.454	090429A	~2.274( $T_{90}$ )	090424	2.016±0.019
090423	2.791±0.022	090419	~2.653( $T_{90}$ )	090418A	2.069±0.017	090417B	3.322±0.016	090407	2.996±0.025
090404	2.384±0.013	090401B	~2.263( $T_{90}$ )	090313	4.448±0.010	090123	~2.117( $T_{90}$ )	090111	2.975±0.042
081230	2.419±0.020	081222	3.038±0.020	081221	2.271±0.009	081210	2.703±0.024	081203A	~2.468( $T_{90}$ )
081128	2.688±0.029	081127	2.567±0.020	081118	2.971±0.045	081109	~2.279( $T_{90}$ )	081102	3.151±0.013
081028	3.807±0.016	081024	≥2.383	081008	2.642±0.009	081007	2.315±0.039	080928	2.635±0.004
080919	≥2.852	080916A	2.232±0.069	080906	2.913±0.023	080905B	2.244±0.024	080810	2.507±0.013
080805	2.444±0.036	080727A	≥3.017	080721	5.214±0.049	080707	2.238±0.039	080613B	2.412±0.013
080607	2.309±0.004	080603B	2.164±0.021	080602	2.146±0.021	080523	~2.009( $T_{90}$ )	080506	2.790±0.014
080503	≥2.888	080413A	2.208±0.039	080328	2.191±0.016	080325	2.689±0.148	080320	2.685±0.020
080319D	2.957±0.028	080319A	≥4.894	080310	4.966±0.043	080307	~2.100( $T_{90}$ )	080229A	2.293±0.008
080212	2.693±0.005	080210	≥5.031	080207	~2.531( $T_{90}$ )	080205	2.267±0.016	080123	2.572±0.031
080120	≥4.183	071227	2.704±0.053	071118	2.958±0.024	071112C	3.082±0.041	071031	3.062±0.025
071028A	2.752±0.044	070808	3.327±0.061	070724A	2.528±0.060	070721B	2.594±0.005	070704	2.719±0.036
070621	2.583±0.033	070616	3.078±0.083	070611	3.633±0.035	070529	2.219±0.018	070520B	2.666±0.024
070520A	2.297±0.077	070518	2.553±0.039	070429A	2.818±0.021	070420	2.306±0.013	070419B	2.588±0.017
070419A	2.846±0.067	070412	1.942±0.041	070318	~1.873( $T_{90}$ )	070311	≥5.689	070306	2.565±0.027
070224	2.950±0.065	070220	~2.111( $T_{90}$ )	070208	3.722±0.042	070129	3.168±0.020	070110	4.535±0.036
070107	2.721±0.010	061222B	2.619±0.087	061222A	2.331±0.014	061202	2.605±0.027	061121	2.328±0.014
061110A	2.747±0.107	061102	2.269±0.084	061028	2.817±0.037	061006	2.548±0.112	060929	3.141±0.032
060906	2.525±0.025	060904B	2.495±0.006	060814	2.856±0.055	060801	≥2.754	060729	4.569±0.006
060719	2.080±0.065	060714	2.453±0.023	060708	2.356±0.034	060614	2.667±0.032	060607A	4.673±0.159
060604	2.380±0.005	060526	≥5.497	060522	2.404±0.033	060512	2.580±0.042	060510B	2.767±0.010
060510A	2.124±0.034	060502A	2.324±0.034	060428B	2.833±0.022	060428A	2.014±0.038	060418	2.294±0.012
060413	3.022±0.030	060306	2.193±0.054	060219	2.348±0.028	060218	4.073±0.017	060211A	2.665±0.080
060210	2.644±0.007	060204B	2.626±0.007	060202	3.096±0.028	060124	2.980±0.001	060115	3.011±0.041
060111B	2.141±0.031	060111A	2.721±0.018	060109	2.382±0.036	051210	≥2.750	051117A	4.358±0.023
051016B	2.132±0.039	051016A	2.446±0.052	051001	3.129±0.031	050922C	2.689±0.029	050922B	3.229±0.012
050915B	2.637±0.023	050915A	2.339±0.046	050904	≥5.498	050822	2.944±0.025	050819	2.827±0.046
050814	2.957±0.022	050803	3.772±0.010	050730	2.853±0.011	050726	4.061±0.040	050724	2.895±0.020
050716	2.819±0.024	050713B	2.604±0.160	050713A	2.506±0.027	050502B	≥5.427	050421	≥2.796
050406	2.560±0.044	050319	2.555±0.029	050315	2.306±0.081				